Received: 3 October 2019 | Revised: 4 November 2019 | Accepted: 7 November 2019

DOI: 10.1002/mdp2.118

WILEY

SPECIAL ISSUE ARTICLE

Effect of strut cross section and strut defect on tensile properties of cubic cellular structure

Sunil Raghavendra[1] | Alberto Molinari[1] | Vigilio Fontanari[1] | Michele Dallago[1] | Valerio Luchin[2] | Gianluca Zappini[2] | Matteo Benedetti[1]

[1]Department of Industrial Engineering, University of Trento, Trento, Italy

[2]Eurocoating S.p.A, Ciré-Pergine (TN), Italy

Correspondence
Sunil Raghavendra, Department of Industrial Engineering, University of Trento, Via Sommarive 9, Trento 38123, Italy.
Email: sunil.raghavendra@unitn.it

Funding information
Eurocoating S.p.A. (Trento, Italy), Grant/Award Number: Contract dated November 6, 2015, between Eurocoati; Provincia Autonoma di Trento (Regional Public Authority)

Abstract

Selective laser melting (SLM) process is used to produce complex geometries for various applications such as biomedical and aerospace industries. However, one of the limitations with respect to this process is the introduction of geometrical defects during the manufacturing process. The presence of these defects makes it difficult to predict their mechanical behaviour. The present work focuses on the cubic lattice structures and their geometrical deviations from the as-designed structures caused by defects like strut oversizing, varying thickness, and strut waviness. The defects were introduced in finite element modelling by using different cross-sections along a strut and joining them to form smooth solid struts. The modelling of defects was validated by comparing with experimental data. The results indicate an appreciable difference between as-designed and as-built structures. It was observed that varying the strut thickness had a major effect on the strength of the structures. Additionally, an elliptical cross-section better matched the tensile behaviour of the as-built structures rather than a rectangular cross-section.

KEYWORDS

finite elements, geometric defects, selective laser melting, tensile test

1 | INTRODUCTION

Cellular structures have a widespread application in various fields of engineering due to their capability to achieve tailored properties according to the loading conditions. They are useful in structural optimization, weight, and cost reduction. Additive manufacturing (AM) process such as electron-beam melting (EBM) and selective laser melting (SLM) have made manufacturing of cellular structures with complex topologies feasible. Development of the AM process has influenced the advancement of cellular structures for biomedical applications where the required stiffness value ranges from 3 to 20 GPa. The SLM process has been validated to have better accuracy when compared with other AM process used for metals.[1] Complex geometries such as gyroid, rhombicuboctahedron, and random structures manufactured using SLM process have been studied.[2–4] Characterization of these cellular structures was carried out using static compression and compression-compression fatigue tests. The tensile behaviour of these samples is considered to be important for structural as well as biomedical applications.[5,6]

In spite of being one of the most preferred AM processes, SLM has some disadvantages such as internal porosity, residual powder, and geometric imperfections. Effects of process parameters such as printing direction, laser power, and scanning distance on build quality and mechanical properties have been studied.[7–9] Investigations have been carried out on the effect of process defects on mechanical properties of cellular structures.[10] Influence of geometric defects on static and fatigue properties has been carried out experimentally as well as using finite element modelling.[11,12] Different modelling techniques have been adopted to model geometric defects, like beam elements,[2,11,13] μCT technique,[14] revolution of spine,[15] and merging of spheres of different diameter.[12] However, revolution of spine and beam element techniques was not able to capture

deviation of strut centroids and variation of strut cross-sections. The merging of spheres captures centroidal deviations along two planes but does not capture the variation of strut cross-sections. While μCT technique is able to model the printed samples accurately, it requires additional experimental work to procure and process the μCT data.

In this current work, we focused on introducing geometric defects such as strut oversizing, varying thickness, and strut waviness into a finite element model of a cubic cell using solid elements. Various geometrical strategies were employed for modelling these defects. The resulting models were subjected to tensile loading and compared with the experimental results in order to identify the better modelling strategy.

2 | MATERIALS AND METHODS

2.1 | Specimen details

A simple stretching dominated cubic cellular structure was considered in order to estimate the geometrical defects. Figure 1A shows the as-designed cubic cellular structure with a wall thickness of 200 μm, a pore size of 1500 μm, and square cross-section. The specimens were manufactured by SLM process using a Renishaw AM250 SLM machine. Atomized titanium alloy (Ti6Al4V) powders were processed at a laser power of 200 W to form 60-μm layers. The manufactured specimens were heat treated at Eurocoating under proprietary conditions in order to relieve residual stresses and transform the martensitic as-built microstructure. The relative density of the samples (ρ/ρ_s) was defined by the total volume of the structure divided by the volume of the solid, which was approximately 7% (93% porosity) for the as-designed structure.

The manufactured samples (as-built structures) were inspected through porosity and morphological analysis, following the experimental procedures described in our previous work.[16] Figure 1B,C shows images of as-built structures perpendicular and parallel to the printing direction that were captured using JEOL JSM-IT300LV scanning electron microscopy (SEM). The images were later analysed using ImageJ analysis software to calculate strut thickness and centre offset along three different axes.

2.2 | Tensile testing and finite element modelling

The tensile test specimens are shown in Figure 2A. The specimen consisted of a cellular part at the centre attached to the solid grips with a fillet in between to avoid failure at their junction. Along with the cellular structures, bulk material was also tested using a circular cross-section dog-

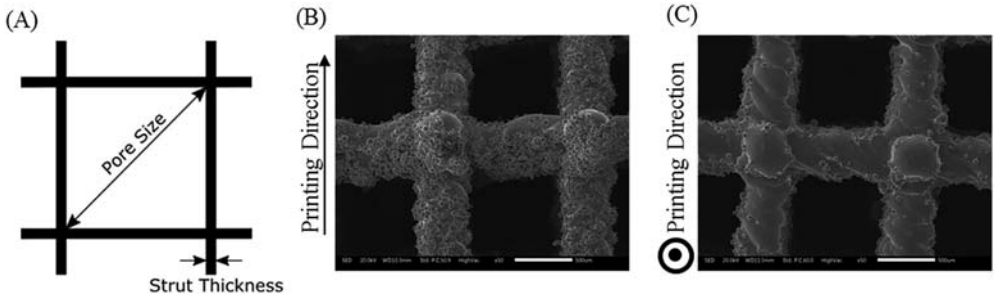

FIGURE 1 A, Schematic representation of pore size and strut thickness; B, view perpendicular to printing direction; C, view parallel to printing direction

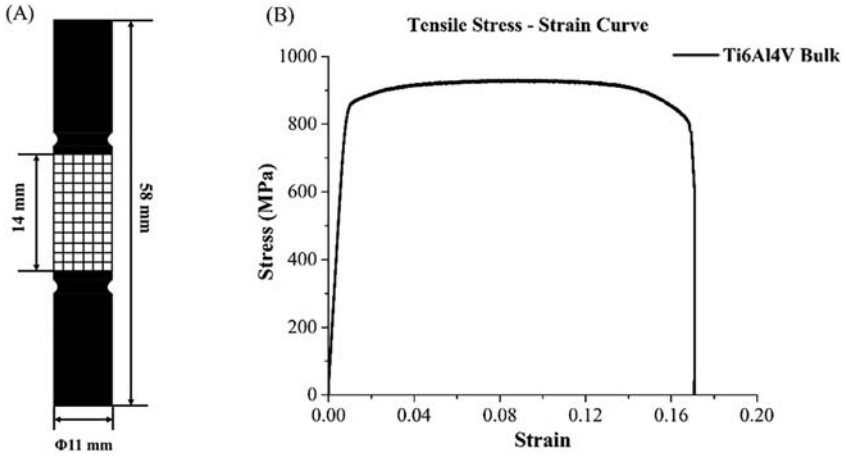

FIGURE 2 A, Schematic representation of cellular structure tensile test specimen; B, stress-strain curve of bulk material manufactured using same selective laser melting (SLM) process

bone shape specimen manufactured using the same SLM process. The tensile tests were conducted on an Instron universal testing machine at a constant crosshead speed of 1 mm/min and a sampling rate of 1 kHz. The displacement in tension was measured using a 12.5-mm Instron extensometer. Data acquisition was carried out using a series IX and SAX V9.3 software. A total of three specimens with cellular structures were tested, while five specimens were tested with bulk material. Average values of Young modulus and yield strength, calculated at 0.2% of strain, were calculated from the tested specimens.

The CAD models for finite element analysis were developed using Inventor (Autodesk). The following defects were incorporated into the as-designed FE models; strut oversizing, strut waviness, and strut centre offset. Two different cross-sections were used, elliptical and rectangular. A detailed discussion about the same is provided in the next section. Finite element models were generated using 10 noded tetrahedron elements of size 0.008 mm in Hypermesh V12. FE model consisted of a 5×5×5 cellular structure with 125-unit cells. Periodic boundary conditions were applied to check for boundary effects. Since no boundary effects were observed, displacement based analysis was carried out by fixing the bottom surface and applying a displacement at the top surface, followed by postprocessing using ANSYS V16. A multilinear elastic-plastic material model was considered using the tensile test data of the bulk specimen shown in Figure 2B, with Young modulus of 109 GPa and Yield strength of 837 MPa. In order to verify that the material properties of bulk material and cellular structures are same, Vickers microhardness test was carried out on both the specimens. The hardness value for cellular structures was 347 ± 14.56, and the bulk specimen was 351 ± 11.24, which confirm the material used was same for both the cases.

3 | STRUT DEFECT ANALYSIS

3.1 | Measurement

The as-designed structure had a pore size of 1500 μm and a strut thickness of 200 μm with a rectangular cross-section as shown in Figure 1A. The SEM images of the as-built cellular structures indicated a clear geometrical deviation, which can be classified into three categories,[2] strut oversizing, strut thickness variation, and strut waviness, as in Figure 3.

The measurements were carried out on 15 struts by taking up to 10 to 12 measurements for each strut. Images were captured along X, Y, and Z directions to evaluate the variations in all the directions. Larger deviations were observed in struts parallel to the printing direction, which is explained in Section 4. Table 1 represents the geometrical deviations such as thickness and centre offset along the struts. The thickness values

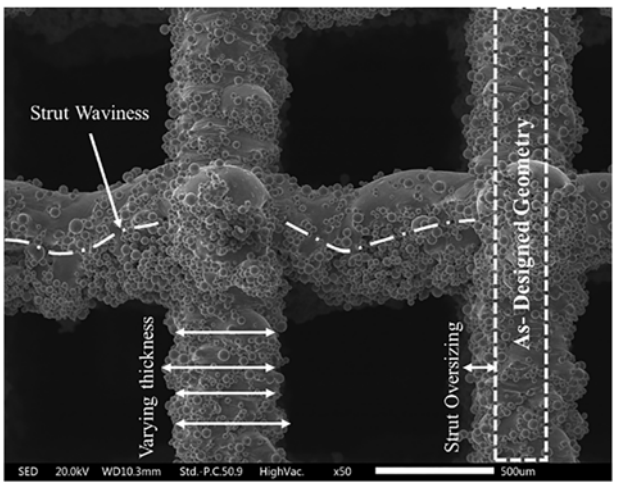

FIGURE 3 Geometrical defects in the as-built specimen

TABLE 1 Measured thickness and centre offset of struts along all the directions

	Measured Thickness, μm			Offset in Centre, μm		
Direction	X	Y	Z	X	Y	Z
Average	447	410	504	11.1	6.7	19.5
Standard deviation	26	55	77	7.7	4.3	9.9
Max value	494	547	665	21.8	11	34
Min value	390	298	334	2	0.2	10

along the X and Y direction are approximately twice the thickness value of the as-built structures. The maximum deviation was measured along Z-direction in the struts that are printed parallel to the printing direction. This deviation was due to the sagging of molten metal under gravitational pull.

3.2 | Geometric models with defects

This section explains in detail the procedure followed to incorporate the defects mentioned in Section 3.1. The defects were introduced into the CAD model in three different stages in order to study the effect of different defects. The modelling was carried out by using elliptical and rectangular cross-sections in all the three directions as shown in Figure 4A. A 5×5×5 model was generated from a unit cell created as described below:

1. As-designed: These models were obtained directly from the STL files used to manufacture the samples. They were rectangular in cross-section and had thickness and pore size as shown in Figure 1A.
2. Average dimensions (AD): The struts had a uniform cross-section, with a mean diameter corresponding to the measured average values (Table 1) along its complete length as shown in Figure 4B. Unlike the sections shown in Figure 4A, only one section was considered in this case, since the thickness remains same along the strut. Struts perpendicular to the printing plane had a lower thickness when compared with the struts parallel to the printing plane as shown in Table 1.
3. Varying cross-section (VCS): In order to model the strut thickness variation, the single measurements performed along ten different sections of the strut (par. 3.1) were employed. These thickness variations are incorporated into the CAD model as shown in Figure 4A in all three directions. The centres of all the sections considered are aligned along a single line. The final model of struts with varying thickness is shown in Figure 4C.
4. VCS with offset: This model introduced strut oversizing, thickness variation, and strut waviness. The modelling was similar to VCS as explained before, but the centres of the sections were offset in order to consider the centroidal offset along the struts. The final CAD is as shown in Figure 4D.

The models were generated using both elliptical and rectangular cross-sections to compare the results of original and printed cross-sections with experimental data.

4 | RESULTS AND DISCUSSION

To verify the accuracy of the modelling process, the results were compared in both elastic and plastic regions. Figure 5A compares Young modulus of the experimental values for both the cross-sections. It was seen that elliptical cross-section underestimates Young modulus, while rectangular cross-section overestimates it. In both cases, modulus decreased with an increase in the number of strut defects introduced (that is, from AD to VCS to VCS with offset)[2,17] The experimental Young modulus of 12.38 GPa lies between the least value of 10.37 GPa from elliptical cross-section and 13.14 GPa from the rectangular cross-section. The values in both cases are extremely high when compared with as-designed Young modulus of 2.88 GPa.

The stress-strain curves of the finite element models were compared with experimental curves as shown in Figure 6A,B. The offset yield strength results are as shown in Figure 5B. Apart from the as-designed model, which largely underestimated the yield strength, all models showed higher values than the experimental data. This could be due to the fact that other defects such as discontinuous struts, and missing struts were not considered in this study. A clear decrease in the yield strength was seen by using VCS along the struts (VCS model) and centre offset (VCS with offset). The curves also indicated that the experimental results were closer to the elliptical cross-section results with an error of 2% while that of the rectangular cross-section was 23%.

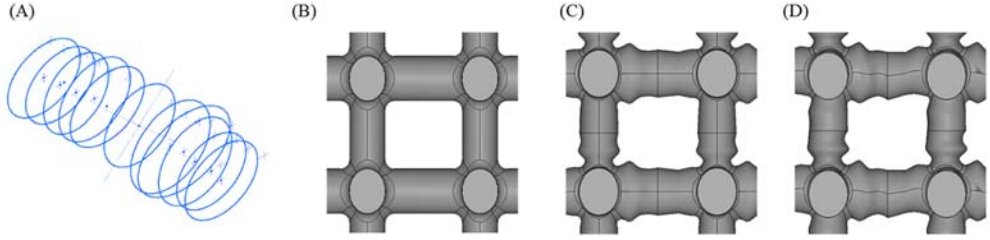

FIGURE 4 Elliptical cross-section A, Ellipse with varying dimensions and centre offset used for CAD modelling; B, CAD model with average dimension (AD); C, CAD model with varying cross-section (VCS); D, CAD model with VCS and centre offset (VCS with offset)

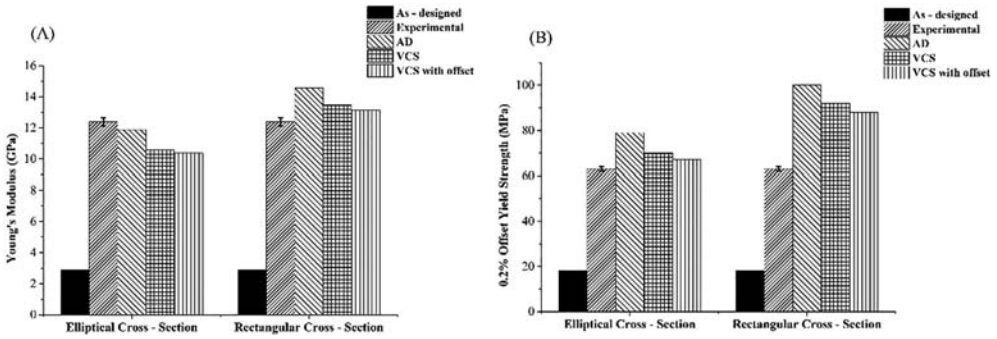

FIGURE 5 Comparison of A, Young modulus and B, offset yield strength of elliptical and rectangular cross-section models with as-designed and experimental values

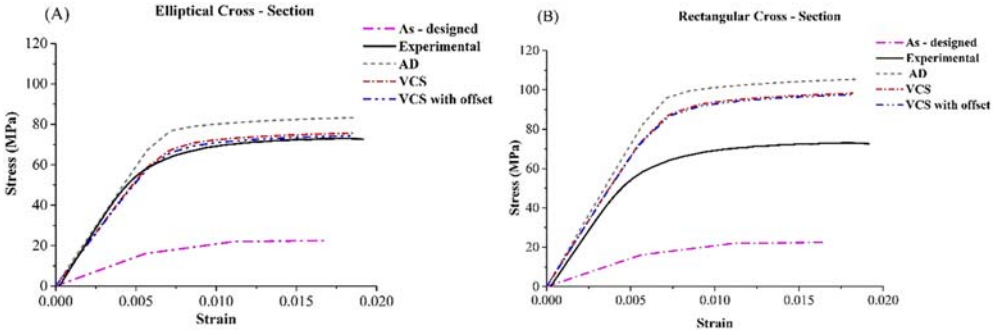

FIGURE 6 Comparison of stress-strain curves for A, elliptical cross-section; B, rectangular cross-section models with as-designed FEM and as-built experimental curve

Generally speaking, by taking into consideration both Young modulus and yield strength, the elliptical cross-section is able to better models the experimental data. Regarding the three modelling strategies (AD, VCS, and VCS with offset), the first one better models the Young modulus, while the third one is closer to the experimental yield strength. The second strategy (VCS) might be a good compromise for predicting both Young modulus and yield strength in one model.

The following considerations shall be done regarding the reasons for the presence of the observed and modelled defects. The discrepancy between the thickness of "as-designed" CAD model and the experimental data shown in Table 1 is related to different process parameters such as layer thickness and laser offset (distance between the designed object contour and real laser path). In case of objects with small dimensions, such as those related to strut thickness, the final effect is an oversizing. This, in turn, increases the stiffness of actual constructs, as evidenced by the difference in Young modulus between as-designed and experimental values. A second cause is related to powder dimension and other laser parameters such as laser spot size, speed, and energy. These affect the final contouring of the struts, leading to a rough surface. Some semi-molten particles remain also attached to the surface, as seen in Figure 3. The third cause is associated with the fact that horizontal struts (perpendicular to printing direction) are built on loose powder, and they tend to "bend" in the middle, as seen in Figure 3. Together with the second cause, this also leads to a VCS of struts and to offset of the node centres.

Diversely from the first cause, the second and third causes act in the opposite manner: They decrease stiffness and strength of constructs. This is because of rough surfaces, semi-molten powders, variation of cross-section, and bent struts act as weak points for the initiation of deformation, stretching, and bending of the whole structure, which have been considered in the modelling process

5 | CONCLUSION

In this study, cubic cellular structure with an as-designed porosity of approximately 93% was manufactured using the SLM process. Geometrical defects were observed in the cellular structures after manufacturing, leading to a decrease in the porosity values to 76%. SEM was used to evaluate the strut thickness and strut waviness in the as-built specimen. To study the effect of different defects, various strategies for generating solid CAD models were studied: shape of cross-section (elliptical or rectangular), mean strut thickness (uniform or variable), and strut axis (straight-lined or waved). Tensile test results from FE modelling were compared with the experimental results, revealing that modelling of structures by considering elliptical cross-sections with varying thickness along the struts can lead to CAD models closer to as-built structures. Future development in this work would be to introduce a correction factor for the geometrical deviations obtained due to the SLM process.

ACKNOWLEDGEMENTS

This work is part of the FAMAC Research Project, cosponsored by Eurocoating S.p.A. and Provincia Autonoma di Trento (Regional Public Authority).

CONFLICT OF INTEREST

The authors declare that they have no conflict of interest.

ORCID

Sunil Raghavendra https://orcid.org/0000-0002-6051-2118
Michele Dallago https://orcid.org/0000-0002-3836-7583
Matteo Benedetti https://orcid.org/0000-0001-9158-2429

REFERENCES

1. Tan XP, Tan YJ, Chow CSL, Tor SB, Yeong WY. Metallic powder-bed based 3D printing of cellular scaffolds for orthopaedic implants: a state-of-the-art review on manufacturing, topological design, mechanical properties and biocompatibility. Materials Science and Engineering: C. 2017;76:1328-1343. https://doi.org/10.1016/j.msec.2017.02.094
2. Liu L, Kamm P, García-Moreno F, Banhart J, Pasini D. Elastic and failure response of imperfect three-dimensional metallic lattices: the role of geometric defects induced by Selective Laser Melting. Journal of the Mechanics and Physics of Solids. 2017;107:160-184. https://doi.org/10.1016/j.jmps.2017.07.003
3. Mullen L, Stamp RC, Fox P, Jones E, Ngo C, Sutcliffe CJ. Selective laser melting: a unit cell approach for the manufacture of porous, titanium, bone in-growth constructs, suitable for orthopedic applications. II. Randomized structures. J Biomed Mater Res Part B Appl Biomater. 2010;92B(1):178-188. https://doi.org/10.1002/jbm.b.31504
4. Bobbert FSL, Lietaert K, Eftekhari AA, et al. Additively manufactured metallic porous biomaterials based on minimal surfaces: a unique combination of topological, mechanical, and mass transport properties. Acta Biomaterialia. 2017;53:572-584. https://doi.org/10.1016/j.actbio.2017.02.024
5. Pazzaglia UE, Ghisellini F, Barbieri D, Ceciliani L. Failure of the stem in total hip replacement—a study of aetiology and mechanism of failure in 13 cases. Archives of Orthopaedic and Trauma Surgery. 1988;107(4):195-202.
6. Andriacchi TP, Galante JO, Belytschko T, Hampton S. A stress analysis of the femoral stem in total hip prostheses. The Journal of Bone and Joint Surgery. American Volume. 1976;58(5):618-624.
7. Edwards P, Ramulu M. Effect of build direction on the fracture toughness and fatigue crack growth in selective laser melted Ti-6Al-4 V. Fatigue and Fracture of Engineering Materials and Structures. 2015;38(10):1228-1236. https://doi.org/10.1111/ffe.12303
8. Qiu C, Yue S, Adkins NJE, et al. Influence of processing conditions on strut structure and compressive properties of cellular lattice structures fabricated by selective laser melting. Materials Science and Engineering A. 2015;628:188-197. https://doi.org/10.1016/j.msea.2015.01.031
9. Wauthle R, Vrancken B, Beynaerts B, et al. Effects of build orientation and heat treatment on the microstructure and mechanical properties of selective laser melted Ti6Al4V lattice structures. Additive Manufacturing. 2015;5:77-84. https://doi.org/10.1016/j.addma.2014.12.008
10. Hernández-Nava E, Smith CJ, Derguti F, et al. The effect of defects on the mechanical response of Ti-6Al-4V cubic lattice structures fabricated by electron beam melting. Acta Materialia. 2016;108:279-292.
11. Dallago M, Winiarski B, Zanini F, Carmignato S, Benedetti M. On the effect of geometrical imperfections and defects on the fatigue strength of cellular lattice structures additively manufactured via selective laser melting. International Journal of Fatigue. 2019;124:348-360. https://doi.org/10.1016/j.ijfatigue.2019.03.019
12. Karamooz Ravari MR, Nasr Esfahani S, Taheri Andani M, et al. On the effects of geometry, defects, and material asymmetry on the mechanical response of shape memory alloy cellular lattice structures. Smart Materials and Structures. 2016;25. Epub ahead of print 2016(2):14, 025008. https://doi.org/10.1088/0964-1726/25/2/025008
13. Campoli G, Borleffs MS, Amin Yavari S, Wauthle R, Weinans H, Zadpoor AA. Mechanical properties of open-cell metallic biomaterials manufactured using additive manufacturing. Materials and Design. 2013;49:957-965. https://doi.org/10.1016/j.matdes.2013.01.071
14. Amani Y, Dancette S, Delroisse P, Simar A, Maire E. Compression behavior of lattice structures produced by selective laser melting: X-ray tomography based experimental and finite element approaches. Acta Materialia. 2018;159:395-407. https://doi.org/10.1016/j.actamat.2018.08.030
15. Karamooz Ravari MR, Kadkhodaei M, Badrossamay M, Rezaei R. Numerical investigation on mechanical properties of cellular lattice structures fabricated by fused deposition modeling. International Journal of Mechanical Sciences. 2014;88:154-161. https://doi.org/10.1016/j.ijmecsci.2014.08.009
16. Raghavendra S, Molinari A, Fontanari V, Luchin V, Zappini G, Benedetti M. Effect of porosity and cell topology on elastic-plastic behavior of cellular structures. Procedia Structural Integrity. 2019;18:93-100. https://doi.org/10.1016/j.prostr.2019.08.143
17. Lozanovski B, Leary M, Tran P, et al. Computational modelling of strut defects in SLM manufactured lattice structures. Materials and Design. 2019;171:18, 107671. https://doi.org/10.1016/j.matdes.2019.107671

How to cite this article: Raghavendra S, Molinari A, Fontanari V, et al. Effect of strut cross section and strut defect on tensile properties of cubic cellular structure. *Mat Design Process Comm*. 2019;e118. https://doi.org/10.1002/mdp2.118